La Soufriere volcanic eruptions launched gravity waves into Space

Jia Yue[1,2], Steven D. Miller[3,4], William Straka[5], Yoo-Jeong Noh[3], Min-Yang Chou[1,2], Ralph Kahn[1], Verity Flower[6]

1. NASA Goddard Space Flight Center, Greenbelt, MD, USA
2. Physics Department, Catholic University of America, Washington, DC, USA
3. Cooperative Institute for Research in the Atmosphere, Colorado State University, Fort Collins, CO, USA
4. Department of Atmospheric Science, Colorado State University, Fort Collins, CO, USA
5. Cooperative Institute for Meteorological Satellite Studies, University of Wisconsin Madison, Madison, WI, USA
6. University of Stirling, UK

Key Points:

1. **La Soufriere volcanic explosive eruptions in April 2021 excited gravity waves propagating into the mesopause.**
2. **MISR detected elevated ash plume after the eruption that overshot the tropopause.**
3. **Concentric ionospheric disturbances in GNSS TEC data could be induced by the volcanic excited gravity waves.**

Abstract

Atmospheric gravity waves can be excited by explosive volcanic eruptions and may reach Earth's upper atmosphere. In this paper, we report on mesoscale concentric gravity waves observed in the mesopause airglow layer following the La Soufriere volcano eruption in April 2021. A large ash plume observed by the spaceborne Multi-angle Imaging SpectroRadiometer (MISR)

instrument on April 10 reached ~20 km. Temporal evolution of the volcanic ash plume was provided by the GOES-16 Advanced Baseline Imager (ABI). Nightglow gravity waves were observed by the Visisble Infrared Imaging Radiometer Suite (VIIRS) Day Night Band (DNB). These waves had horizontal wavelengths of ~25-40 km, and took about a half-to-one hour to travel from the tropopause to the mesopause. Some concentric ionospheric disturbance signatures are also seen in GNSS-TEC (total electron content) maps. We found the launch of gravity waves to be highly correlated with the elevated ash plume from explosive eruptions.

Plain language summary

Explosive volcanic eruptions occur when the pressure of hot gases trapped inside magma builds up, resulting in the rapid injection hot gas and ash many kilometers into the atmosphere, sometimes reaching the stratosphere. Atmospheric gravity waves are excited in this process. Concentric gravity waves observed in the mesopause airglow layer were launched by the La Soufriere volcano explosive eruption in April 2021. A large ash plume on April 10 reached ~20 km, overshooting the tropopause layer. Nightglow gravity waves observed by the Day Night Band of VIIRS instruments on both the Suomi NPP and NOAA-20 satellites reveal concentric patterns. These waves took about a-half-to-one hour to reach the mesopause. Some concentric ionospheric disturbance signatures are also induced by the volcanic gravity waves. Our observations of this event provide direct evidence of lithosphere-atmosphere-ionosphere coupling via the generation and propagation of gravity waves.

1. Introduction

Volcanic eruptions become explosive when hot gases are trapped inside magma and pressure gradually build up. Explosions occur when the gases blast out of vent violently,. issuing hot gases and ash kilometers into the atmosphere, sometimes reaching the lower stratosphere. Gravity (or buoyancy) waves arise from departures of air from its equilibrium in a stably stratified background atmosphere such as in the stratosphere. Buoyancy under stable stratification acts as the restoring force for these waves. Explosive volcanic eruptions along with hot ash can drastically perturb air in the troposphere and stratosphere, thus exciting a broad spectrum of gravity waves, in addition to acoustic waves.

Gravity and infrasonic (acoustic) waves have been observed near the ground after large volcanic eruptions. Barogram and seismogram recordings during the eruptions of El Chichon in 1982 and Mount Pinatubo in 1991 measured both near-field and far-field Rayleigh waves and infrasonic-acoustic waves having periods of a few hundred seconds, i.e., mHz frequency (Mauk, 1983; Kanamori & Mori, 1992; Widmer & Zurn, 1992; Tahira et al., 1996). Acoustic coupling with the air waves excited by the eruptions was suggested to be the source of those Rayleigh waves. Both infrasonic and gravity waves have been detected in the near field (< 6 km) by an infrasonic array and pressure transducers near the Soufriere Hills Volcano, Montserrat (Ripepe et al., 2010). In particular, gravity waves with frequencies as low as ~ 1 mHz or 1000 s (~16 min) periods have been recorded during volcanic eruptions (De Angelis et al., 2011). Volcanic eruption-excited air waves are postulated as being the response of the atmosphere to mass or heat injections at a single point source (Kanamori et al., 1994; Baines & Sacks, 2017). As such, Ripepe et al. (2016) suggest using the gravity waves generated by volcanic eruptions near the source to deduce the size, rate and duration of eruptions. All prior observations and hypotheses

68 considered only near-surface volcanic gravity waves—not upward propagating waves as
69 observed in the current study.

70 The ionosphere begins about 80 km above the surface, an atmospheric layer where
71 molecules and atoms are weakly ionized. Disturbances in ionospheric density or total electron
72 content (TEC) by explosive volcanic eruptions, so-called covolcanic ionospheric disturbances
73 (CVID), have been observed 10-45 min after several large events (Astafyeva, 2019). CVIDs
74 were observed after the eruption of Mount St. Helens on May 18 1980 (Roberts et al., 1982a,
75 1982b; Ogawa et al., 1982) and Mount Pinatubo on 15 June 1991 along with surface pressure
76 fluctuations (Cheng & Huang, 1992; Igarashi et al., 1994). These CVIDs had periods of 16-30
77 min, wavelengths of 160-435 km and velocities of 131-290 m/s. Heki (2006) detected CVIDs
78 with electron column densities of 0.03-0.16 TECU 12 min after the 1 September 2004 Asama
79 volcano explosion in Japan. Dautermann et al. (2009) found quasiperiodic CVIDs with a period
80 of ~ 12 min that lasted 40 min after the Soufriere Hill Volcano in Montserrat erupted on 13 July
81 2003. Furthermore, Manta et al. (2021) defined the Ionospheric Volcanic Power Index (IVPI) to
82 quantify the relationship between the TEC perturbation and the volcanic eruption characteristics.
83 Although many of the observed CVIDs were associated with gravity waves, Most of the
84 observed CVIDs were apparently caused by acoustic waves with shorter periods, higher
85 frequencies, and faster velocities (e.g., Heki, 2006; Shults et al., 2016; Nakashima et al., 2016);
86 rare cases have been clearly associated with gravity waves. Acoustic waves are outside the scope
87 of this paper.

88 There have also been only rare observations of gravity waves between the ground and the
89 ionosphere excited by volcanic eruptions, prohibiting a thorough understanding of their
90 excitation and vertical propagation. The single definite volcanic gravity wave observation in the

mesopause region (~85 km) was made over the 23 April 2015 Calbuco volcano eruption (41°S, 72°W) in Chile using the Day/Night Band (DNB) of the Visible Infrared Imaging Radiometer Suite (VIIRS) imager on the Suomi National Polar-orbiting Partnership (NPP) satellite (Miller et al., 2015). Along with the volcanic ash plume observed in the VIIRS 10.76 μm infrared imagery, the DNB revealed concentric gravity waves centered over the volcano. This ring pattern in nightglow was reminiscent of gravity waves launched from deep convection (e.g., Taylor and Hapgood, 1988; Sentman et al., 2003; Suzuki et al., 2007; Yue et al., 2009, 2014; Miller et al., 2015; Smith et al., 2020). It suggests that they might be attributed to similar excitation mechanisms: rapid mechanical "overshooting" of the tropopause and sudden heating, in this case ash/gas heating from volcanic eruptions rather than latent heating within thunderstorms (Fritts & Alexander, 2003). However, no detailed analysis has so far been carried out on volcanic gravity wave (GW) events in the middle atmosphere.

On the other hand, there have been independent CVID reports on this same Calbuco eruption event (Shults et al., 2016; Liu et al., 2017). Shults et al. (2016) reported two types of CVIDs, the first group occurred ~15 min after the initial eruption and the second group ~40 min after the second eruption. All modes were acoustic waves that propagated at the sound speed of 0.8-1 km/s in the ionosphere (Shults et al., 2016). There is a missing link between the mesopause and ionosphere for the gravity waves excited by the 2015 Calbuco eruption. Furthermore, no study connects the heat released from the tropospheric/stratospheric volcanic plume or explosion to nightglow waves in the mesopause region and then upward to CVIDs in the ionosphere. It is extremely challenging to observe nightglow volcanic gravity waves from the ground, as the ash plume can obscure optical observations. However, spaceborne airglow-sensitive sensors can

113 detect those waves, provided that the satellite overpass time coincides with the eruption and
114 appearance of the ephemeral wave pattern.

115 In this letter, we report on nightglow gravity waves near the mesopause region from the
116 La Soufriere volcanic eruption that occurred in April 2021 and CVIDs observed in ionospheric
117 TEC. By way of these novel observations, we help fill the outstanding gap between the ground
118 and the ionosphere and shed some light on volcanic gravity wave generation and propagation
119 into the upper atmosphere.

120

121 **2. La Soufriere volcanic eruptions**

122 La Soufriere (13°N, 61°W) is an active stratovolcano on the main island of Saint Vincent and
123 the Grenadines in the Caribbean. The eruption started with an effusive phase on December 27,
124 2020 as its lava dome was growing. The first explosive eruption occurred at 1240 UT (840 AM
125 local time, LT) on 9 April 2021, forcing about 16,000 people to evacuate. The ash plume reached
126 up to 8 km. The second explosion occurred in the afternoon (1445 LT or 1845 UT), followed by
127 a third one at 1845 PM LT or 2245 UT. According to the Global Volcanism Program of
128 Smithsonian Institution/National Museum of National History, "Periods of banded tremor
129 associated with explosive activity and stronger pulses of ash emissions to higher altitudes began
130 at 0330 LT or 0730 UT on 10 April, lasting for periods of 20-30 minutes with 1-3-hour gaps. The
131 resulting ash plumes rose to 10-16 km altitude throughout the day." On 11 April, explosions and
132 ash emissions continued, with associated plumes rising to 12-16 km. The University of East
133 Anglia identified about 30 explosions through 18 April, though most explosions took place
134 during April 9-11. No plumes higher than 12 km were reported after April 11. More information
135 about the La Soufriere eruptions can be found on the website of the Global Volcanism Program

of Smithsonian Institution/National Museum of National History available at https://volcano.si.edu/volcano.cfm?vn=360150. The timelines of volcanic eruption and relevant observations below are summarized in Table 1. Not all ~30 explosions are included.

Events/Observations	Time/Date (UT)	Measurements	Height
First explosion	1240, 9 April	ground	surface, troposphere
Second explosion	1845, 9 April	ground	surface, troposphere
Third explosion	2245, 9 April	Ground	surface, troposphere
Elevated plume	1435, 10 April	MISR	tropopause
One explosion	0300-0320, 11 April	ABI	troposphere
Another explosion	0500-0530, 11 April	ABI	troposphere
lightning	0510, 11 April	GLM	troposphere
Nightglow gravity wave 1	0516, 11 April	VIIRS on SNPP	mesopause
Nightglow gravity wave 2	0606, 11 April	VIIRS on NOAA20	mesopause
CVIDs	0605-0702, 11 April	GNSS TEC	Ionosphere

Table 1. Chronicles of important events observed during the La Soufriere volcanic eruptions in April 2021.

The NASA Disasters Program monitored and reported on this eruption and precursors, based primarily on NASA spacecraft observations and associated modeling, beginning in December 2020:

https://maps.disasters.nasa.gov/arcgis/apps/MapSeries/index.html?appid=483b9f632f6c4dadbb7

3fa60e8b30b4f. On April 10, 2021, the NASA Terra satellite flew over La Soufriere and the Multi-angle Imaging SpectroRadiometer (MISR) instrument (Diner et al., 1998) aboard this platform observed the volcanic plume at 14:35 UT, as shown in Figure 1. Plume 3-D structure, motion vectors, and particle microphysical properties were derived from the MISR multi-angle, multi-spectral imagery, using the MISR Interactive eXplorer (MINX) software developed for this purpose (e.g., Nelson et al., 2013; Flower & Kahn, 2020; Junghenn-Noyes et al., 2020). A user defines the plume outline, source location, and wind direction in on-screen imagery, and the program calculates the heights of contrast features in the plume at 1.1 km horizontal and 250-500 m vertical resolution from the apparent geometric parallax. As it takes about 7 minutes for the nine MISR cameras to view a given location on Earth, the associated wind vectors, along with wind-corrected heights, are also derived. Figure 1a shows the wind-corrected results obtained from MISR red-band imagery.

MISR measurements of La Soufriere volcanic plume are not available on other days. Figure 1a shows that the plume peaked at around 20 km above the volcano, suggesting that some plume material penetrated the tropopause at ~17.5 km (read from the radiosonde at 0 UT on April 10 2021 at station TBPB Grantley Adams Observations, tropopause temperature was -82 C or 191K, https://weather.uwyo.edu/upperair/sounding.html). This plume reached the stratosphere. Recall that the ground-based naked eye observation estimated ash plume rose to “10-16 km altitude” on April 10, significantly lower than the MISR measurement. This is because ground observations offer a different perspective from MISR, often sampling closer to the lower aerosol layers than to the tops, that are more readily observed from space (e.g., Flower and Kahn, 2017). The plume was transported to the east, with significant lateral spreading of 250 km. Bands appear progressively downwind in the imagery, consistent with banded tremors and pulses of ash

emissions. Figure 1b illustrates the vertical structure of the plume in downwind profile, clearly showing that the maximum height is ~20 km. In general, close correlation between convective overshooting of the tropopause by 1-3 km and concentric gravity waves in nightglow at ~85 km has been established previously (Yue et al., 2009; Vadas et al., 2012). Because the stratosphere is stably stratified, mechanical or thermal disturbances in this layer will naturally excite gravity waves with large enough vertical wavelength to penetrate the upper atmosphere and become observable. Though the MISR measurements of the plume vertical structure are available only at one instance on April 10, we speculate that the very high plume injection continued on April 11. Circumstantial evidence supporting this hypothesis is presented next.

To gain more temporal information about the plume, we closely inspect measurements from GOES-16, a next-generation geostationary weather satellite operated by the National Oceanic and Atmospheric Administration (NOAA), on April 11, around the time of nightglow observations discussed in the next section. The Advanced Baseline Imager (ABI) spectral band at 11.2 μm IR on GOES-16 recorded pulsed volcanic plumes from this event (Figure 2). On April 11, one eruption took place around 0300-0320 UT, and a later one was around 0500-0530 UT, accompanied by a blue lightning flash measured by the GLM (Geostationary Lightning Mapper) also on GOES-16 (Figure 2, Panel 3). No eruptions occurred between 0320 and 0500 UT (middle panel of Figure 2). The lightning signal is the accumulation of GLM Level-2 group energy over ABI's scan duration (full-disk 10 minutes for this case). The interval between consecutive eruptions was ~1-2 hours and each eruption lasted 20-30 min. This is consistent with the aforementioned ground observations/records from Global Volcanism Program. Volcanic lightning usually forms in thick volcanic plumes such as the one characterized by MISR (Figure 1) (McNutt and Williams, 2010). As particles are violently ejected into a volcanic plume, they

191 rub against each other and become electrically charged. When charged particles ascend, the
192 plume gains charge separation and lightning occurs. Similar volcanic lightning was also
193 observed from the 2015 Calbuco volcano eruption (Eaton et al., 2016). All the MISR, ABI and
194 GLM measurements suggest that periodic, strong explosions and high plume injection took place
195 on April 10 and 11, likely favoring gravity wave excitation.
196
197 **3. Nightglow gravity waves**
198 Similar to the nightglow gravity waves above the Calbuco volcanic eruption in 2015 (Miller
199 et al., 2015), nightglow concentric gravity waves near Saint Vincent were observed in the DNB
200 of VIIRS on board the Suomi NPP satellite at 0516 UT and aboard the NOAA-20 satellite at
201 0606 UT on April 11, 2021, as shown in Figure 3. The thermal IR (11 μm) band of VIIRS maps
202 volcanic plumes with moderate resolution (750 m/pixel at nadir). The brightness temperature of
203 the ash plume colder than 190 K at 0606 UT in Figure 3, which further confirms that the
204 volcanic plume on April 11 "overshot" the tropopause. The ash/cloud top temperature being
205 colder than the tropopause temperature (194 K at the 18-km tropopause height at 12 UT on April
206 11, 2021) is indicative of tropopause "overshooting" (Yue et al., 2009).
207 VIIRS DNB observations (over 0.5–0.9 μm wavelength) of OH airglow gravity waves were
208 first reported by Miller et al. (2013, 2015) and Yue et al. (2014, 2019). The faint signatures of
209 gravity waves in the airglow can also be seen in DNB/VIIRS of Suomi NPP at 0516 UT on April
210 10 (shown in the appendix). No airglow gravity waves were observed after April 11, consistent
211 with the fact that no high plumes were reported on subsequent days. The apparent centers of
212 these rings are near the volcano. The waves have horizontal wavelengths of ~25-40 km. To
213 estimate the propagation time from the tropopause to the OH airglow layer at ~85 km, we

assume the vertical wavelength is 40 km, twice the elevation of the plume observed by MISR. This conjecture is based on the concept that gravity waves from convective heating can have vertical wavelengths approximately twice the depth of heating (~40 km) or even longer (Holton et al., 2002). As the background wind is typically weak (<20 m/s) in the stratosphere and mesosphere in April (Liu et al., 2021), we assume zero background wind (Yue et al., 2009). Using the gravity wave dispersion relationship of equation 3 in Yue et al. (2009), we estimate the vertical group velocity to be about 20-40 m/s, and the propagation time from the tropopause to mesosphere to be ~30-60 min. Inclusion of a weak background wind will not change this estimate significantly (<10%) because these are fast propagating waves. Therefore, the gravity waves at 0516 UT were excited at ~0416-0446 UT and the waves at 0606 UT originated around 0506-0536 UT. Recall that the closest explosions before 0606 UT took place at 0300-0320 UT and 0500-0530 UT, based on ABI observations. Because ABI recorded no explosions during 0416-0446 UT, the gravity waves observed at 0516 UT could not have been excited by a contemporaneous explosion, but likely by lofting from the high plume after the explosion and "overshooting" of the tropopause (Yue et al., 2009; Vadas et al., 2009) (Figures 1 and 3). On the other hand, the waves at 0606 UT could have been excited by either the elevated plume or the explosion at 0500-0530 UT. As those volcanic gravity waves in the DNB imagery had already reached the mesopause by 0516 UT, they could likely penetrate the ionosphere and perturb plasma densities, as shown in Figure 3.

4. CVIDs

We further examined the ground-based Global Navigation Satellite System (GNSS) TEC observations over the Caribbean to identify any CVIDs, as illustrated in Figure 4. The 30-s sampling of GPS and GLONASS Receiver Independent EXchange (RINEX) data from the dual

frequency receivers operated by Continuously Operating Reference Stations (CORS), Scripts Orbit and Permanent Array Center (SOPAC), and Instituto Brasileiro de Geografia e Estatística (IBGE) are utilized to calculate the vertical TEC. Details of the TEC processing procedures are presented by Liu et al. (1996). Note that we assume the altitude of ionospheric pierce point (IPP) to be 300 km for converting the slant TEC to vertical TEC, and elevation angles greater than 20˚ are excluded to mitigate multipath error. Then, the fifth order Butterworth filter with periods of 10-30 min is applied to extract the TEC perturbations related to CVIDs for each vertical TEC observation.

Figure 4 shows the time sequence of GNSS TEC maps in the immediate vicinity of the La Soufriere volcano during ~0605-0702 UT on April 11, 2021. Mesoscale traveling ionosphere disturbances (TIDs) centered at St. Vincent were only observable to the northwest during 0630-0730 UT on April 11. There are two distinct crests of ~0.08 TEC Unit (TECU) disturbance over Cuba (Figure 4c and 4d). We searched for these CVIDs in TEC near the volcano in April 2021 and cannot find similar perturbations. Figure 4e, the TID keogram, reveals that these CVIDs have phase velocities of ~175-192 m/s, periods of ~21-26 min, and horizontal wavelengths of ~220-300 km, consistent with previous CVIDs. The perturbations of CVIDs are minor owing to the low ionospheric electron density after midnight; however, the CVIDs display a coherent wave pattern emanating northwestward. One challenge is that GNSS receivers are sparse over the Caribbean compared to the continental US, Europe, or Japan. No GNSS measurements over the ocean are available to the east of St. Vincent where nightglow gravity waves are seen.

Though these CVIDs were not caused by the gravity waves seen in VIIRS, both were likely excited by the same volcanic eruption. To test the hypothesis that the observed CVIDs were likely related to gravity waves excited by the La Soufriere volcanic eruption, we can

calculate the horizontal distance travelled by gravity waves from their source using equation 2 in Yue et al. (2009).

$$R = \Delta z \tan\beta = \Delta z \sqrt{\left(\frac{N}{\omega_I}\right)^2 - 1} \quad (1)$$

where Δz and β indicate the vertical distance from the source to the ionosphere and zenith angle between vertical and wave vector, respectively. R is the horizontal distance travelled by gravity waves from their source. N is the Brunt-Väisälä frequency and ω_I is the intrinsic frequency. Assuming Δz=280 km from the plume altitude of 20 km to the IPP altitude of 300 km and N = $\frac{2\pi}{8.8\ min}$ using the empirical neutral atmosphere parameters from NRLMSISE-00 (Picone et al., 2002), the horizontal distance travelled by gravity waves from their source is estimated to be ~606-778 km. This is generally consistent with the TEC observations; the keogram (Figure 4e) shows CVIDs emerging approximately 650 km away from the volcano. The calculated vertical velocity is 68-73 m/s. Thus, the estimated propagation time from the tropopause to the ionosphere (or horizontally from the volcano to the wave front) is about one hour. Therefore, these CVIDs can be associated with volcanic gravity waves excited at ~ 0530-0630 UT, after the explosion of 0500-0530 UT, and the source was likely the elevated ash plume. Because the timing of the sources is different between the CVIDs and nightglow gravity waves, these two waves (nightglow in Figure 3 and CVIDs in Figure 4) were excited by different point sources (either elevated plume or explosion). But they were likely both ultimately associated with the volcano eruption.

5. Discussion and conclusion

Unlike previous volcanic gravity waves, that were measured near-surface, this paper focuses on gravity waves in the mesosphere and ionosphere. This is the second documentation of airglow

283 gravity waves from volcanic eruptions, following the Calbuco eruption in April 2015 (Miller et
284 al., 2015). The common features of both volcanic eruptions are strong explosion level (Volcanic
285 Explosivity Index, VEI≥4) and elevated ash plume production. The Calbuco eruption sent plume
286 particles more than 15 km above the surface, "overshooting" the midlatitude tropopause of ~12
287 km. The gravity wave excitation mechanism closely resembles deep convection with tropopause
288 "overshooting." The absence of nightglow gravity waves after April 11, 2021 confirms that a
289 high-altitude plume is a necessary condition for wave generation. Weak stratospheric and
290 mesospheric winds in the month of April (both Calbuco, 2015 and La Soufriere 2021 eruptions)
291 enables gravity wave propagation to higher altitudes. On the other hand, effusive eruptions, such
292 as commonly occur at Hawaii's Kilauea volcano, produce only surface lava flows. Lacking
293 explosive eruption producing elevated plumes and ash, effusive eruptions are not effective at
294 exciting gravity waves.

295 GNSS soundings have been widely used to study and monitor acoustic and gravity waves
296 from seismic activity, such as earthquakes and tsunamis (Astafyeva, 2019). Such waves are
297 excited by vertical displacements of the ground or ocean floor. However, volcanic eruptions
298 excite gravity waves in a way similar to deep convection or thunderstorms. As most explosive
299 volcanic eruptions in the 21st century have been located in remote areas (settlements tend to
300 avoid these hazardous areas), good GNSS coverage of volcanic eruptions is less likely compared
301 to that for earthquakes and tsunamis. Polar-orbiting satellites such as Suomi NPP and NOAA20
302 have to fly over volcanic eruptions at the right time to capture those airglow gravity waves
303 during night. Therefore, it is challenging to obtain gravity wave data that would provide
304 additional information about eruptions, except for the explosive characteristics and plume
305 elevation that ground observations usually provide (e.g., the United States Geological Survey

(USGS) reports https://www.usgs.gov/programs/VHP). A potential ground-based gravity wave observational campaign could deploy airglow cameras or GPS receivers at nearby but safe locations (several hundreds of km away) before a forecasted volcanic eruption. The La Soufriere volcano was in effusive eruption mode for months before its final explosive eruption phase in April 2021. Such events could give some lead time for field campaign planning.

It is yet more challenging to conduct similar surface observations on other planets or moons than on Earth. However, we postulate that volcanic gravity waves can be a tool to probe active volcanic eruptions on other planetary/lunar bodies in the solar system as well, such as Venus, Io, Triton and Enceladus, whether by radio wave or optical remote sensing. For example, gravity waves have been observed in the Venus atmosphere from Venus Express (Ando et al., 2015; Sugimoto et al., 2021). This airglow volcanic-wave-monitoring idea was also recently postulated by Byrne and Krishnamoorthy (2022).

In summary, this paper provides a novel example of Lithosphere-atmosphere-ionosphere coupling through the generation and propagation of gravity waves. ABI, MISR, GLM, and VIIRS provide temporal and 3D spatial information about the La Soufriere eruption and its plume. The DNB sensor on VIIRS observed the second instance of nightglow gravity waves from a volcanic eruption, following the Calbuco eruption in 2015. The GNSS network measured CVIDs to the northwest of the eruption. We understand now that these gravity waves were most likely excited by elevated eruption plumes reaching above the tropopause rather than by the explosions themselves. We expect more observations of volcanic gravity waves in the mesosphere and ionosphere, leading to enhanced understanding in the future. Numerical simulations combining volcanic eruptions, gravity wave excitation and propagation and their

328 ensuing disturbances in the ionosphere are of prime interest when linking this process to
329 applications such as radio frequency communication impacts.
330
331

Acknowledgement: The MISR contribution to this paper is part of the NASA Active Aerosol Plume-height (AAP) Project, V. Flower, R. Kahn, K. Junghenn-Noyes, visualized by Garrett Layne, NASA Disasters Program. The work of R. Kahn and V. Flower is supported in part by the NASA Earth Surface and Interior program under Ben Phillips and the NASA Atmospheric Composition Program under Richard Eckman. JY and MC are supported by NASA 80NSSC20K0628 and AIM. WCS are supported by the NOAA JPSS and GOES-R program offices via Award No. NA20NES4320003.

Open Data: The volcanic plume height calculation was performed using the MISR INteractive eXplorer (MINX) software tool, which is publicly available at https://github.com/nasa/MINX. MISR data can be accessed at https://misr.jpl.nasa.gov/getData/accessData/. Suomi NPP and NOAA20 VIIRS data, GOES-16 ABI L1b and GLM L2 data are all publicly available at the NOAA Comprehensive Large Array-data Stewardship System (CLASS; https://www.class.noaa.gov), which can be found under "JPSS VIIRS Sensor Data Record Operational (VIIRS_SDR)", "GOES-R Series ABI Products (GRABIPRD)" and "GOES-R Series GLM L2+ Data Product (GRGLMPROD)", respectively. The processed GNSS TEC data is available at https://doi.org/10.5281/zenodo.5855060.

References:

Ando, H., Imamura, T., Tsuda, T., Tellmann, S., Patzold, M., & Hauler, B. (2015). Vertical wavenumber spectra of gravity waves in the Venus atmosphere obtained from Venus Express Radio Occultation Data: Evidence for saturation. Journal of the Atmospheric Sciences, 72(6), 2318–2329. https://doi.org/10.1175/JAS-D-14-0315.1

Astafyeva, E. (2019). Ionospheric detection of natural hazards. Reviews of Geophysics, 57, 1265-1288. https://doi.org/10.1029/2019RG000668.

Baines, P.G., & Sacks, S. (2017). The Generation and Propagation of Atmospheric Internal Waves Caused by Volcanic Eruptions. Atmosphere, 8(3), 60; https://doi.org/10.3390/atmos8030060

Byrne, P. K., & Krishnamoorthy, S. (2022). Estimates on the frequency of volcanic eruptions on Venus. Journal of Geophysical Research: Planets, 127, e2021JE007040. https://doi.org/10.1029/2021JE007040

Cheng, K., & Huang, Y. N. (1992). Ionospheric disturbances observed during the period of Mount Pinatubo eruptions in June 1991. Journal of Geophysical Research: Space Physics, 97(A11), 16995–17004. https://doi.org/10.1029/92JA01462

376 Dautermann, T., Calais, E., & Mattioli, G. S. (2009). Global Positioning System detection and
377 energy estimation of the ionospheric wave caused by the 13 July 2003 explosion of the Soufrière
378 Hills Volcano, Montserrat. Journal of Geophysical Research, 114(B2), B02202.
379 https://doi.org/10.1029/2008JB005722
380
381 De Angelis, S., McNutt, S. R., & Webley, P. W. (2011). Evidence of atmospheric gravity waves
382 during the 2008 eruption of Okmok volcano from seismic and remote sensing observations,
383 Geophysical Research Letters, 38, L10303, doi:10.1029/2011GL047144.
384
385 Diner, D.J., Beckert, J.C., Reilly, T.H., Bruegge, C.J., Conel, J.E., Kahn, R.A., Martonchik, J.V.,
386 Ackerman, T.P., Davies, R., Gerstl, S.A.W. *et al*. (1998). Multi-angle Imaging
387 SpectroRadiometer (MISR) instrument description and experiment overview. *IEEE Transactions*
388 *on Geoscience and Remote* Sensing, *36*, 1072–1087.
389
390 Van Eaton, A. R., Á. Amigo, D. Bertin,L. G. Mastin, R. E. Giacosa, J. González, O. Valderrama,
391 K. Fontijn, and S. A. Behnke(2016), Volcanic lightning and plumebehavior reveal evolving
392 hazards during the April 2015 eruption of Calbucovolcano, Chile, Geophys. Res. Lett., 43,3563–
393 3571, doi:10.1002/2016GL068076.
394
395 Flower, V., and R.A. Kahn, 2017. Assessing the altitude and dispersion of volcanic plumes using
396 MISR multi-angle imaging: Sixteen years of volcanic activity in the Kamchatka Peninsula,
397 Russia. J. Volcanology and Geothermal Research 337, 1–15, doi:
398 /10.1016/j.jvolgeores.2017.03.010.

399

400 Flower, V.J.B., & Kahn, R. A. (2020). The evolution of Iceland volcano emissions, as observed
401 from space. Journal of Geophysical Research: Atmospheres, 125, e2019JD031625,
402 doi:10.1029/2019JD031625.

403

404 Fritts, D. C., & Alexander, M. J. (2003). Gravity wave dynamics and effects in the middle
405 atmosphere, Reviews of Geophysics,41(1), 1003, doi:10.1029/2001RG000106.

406

407 Global Volcanism Program (2021). Report on Soufriere St. Vincent (Saint Vincent and the
408 Grenadines). In: Sennert, S K (ed.), Weekly Volcanic Activity Report, 15 September-21
409 September 2021. Smithsonian Institution and US Geological Survey.

410 Heki, K. (2006). Explosion energy of the 2004 eruption of the Asama Volcano, central Japan,
411 inferred from ionospheric disturbances. Geophysical Research Letters, 33, L14303.
412 https://doi.org/10.1029/2006GL026249

413

414 Holton, J. R., Beres, J. H., & Zhou, X. (2002). On the Vertical Scale of Gravity Waves Excited
415 by Localized Thermal Forcing. Journal of the Atmospheric Sciences, 59(12), 2019–2023.,
416 doi:http://dx.doi.org/10.1175/1520-0469(2002)059<2019: OTVSOG>2.0.CO;2.

417

418 Igarashi, K., Kainuma, S., Nishimuta, I., Okamoto, S., Kuroiwa, H., Tanaka, T., & Ogawa, T.
419 (1994). Ionospheric and atmospheric disturbances around Japan caused by the eruption of Mount
420 Pinatubo on 15 June 1991. Journal of Atmospheric and Terrestrial Physics, 56(9), 1227–1234.
421 https://doi.org/10.1016/0021-9169(94)90060-4

Junghenn, K.T., Kahn, R.A., Limbacher, J.A., Sedlechek, A., Kleinman, L., & Li, Z. (2020). Wildfire Plume Particle Properties and Evolution, From Space-Based Multi-angle Imaging. Biomass Burning special issue. Remote Sensing, 12, 769; doi:10.3390/rs12050769.

Kanamori, H., & Mori, J. (1992). Harmonic excitation of mantle Rayleigh waves by the 1991 eruption of Mount Pinatubo, Philippines. Geophysical Research Letters, 19, 7, 721-724.

Kanamori, H., Mori, J. & Harkrider, D. G (1994). Excitation of atmospheric oscillations by volcanic eruptions. Journal of Geophysical Research: Solid Earth, 99, 21,947–21,961, doi: 10.1029/94JB01475.

Liu, J. Y., Tsai, H. F., & Jung, T. K. (1996). Total electron content obtained by using the Global Positioning System. *Terrestrial, Atmospheric and Oceanic Sciences*, **7**, 107.

Liu, X., Zhang, Q., Shah, M., & Hong, Z. (2017). Atmospheric-ionospheric disturbances following the April 2015 Calbuco volcano from GPS and OMI observations. Advances in Space Research, 60(12), 2836–2846. https://doi.org/10.1016/j.asr.2017.07.007

Liu, X., Xu, J., Yue, J., Yu, Y., Batista, P. P., Andrioli, V. F., Liu, Z., Yuan, T., Wang, C., Zou, Z., Li, G., & Russell III, J. M. (2021). Global Balanced Wind Derived from SABER Temperature and Pressure Observations and its Validations. Earth System Science Data, https://doi.org/10.5194/essd-2021-192, in press.

Manta, F., Occhipinti, G., Hill, E. M., Perttu, A., Assink, J., & Taisne, B. (2021). Correlation between GNSS-TEC and eruption magnitude supports the use of ionospheric sensing to complement volcanic hazard assessment. Journal of Geophysical Research: Solid Earth, 126(2), e2020JB020726-. https://dx.doi.org/10.1029/2020JB020726

Mauk, F. J. (1983). Utilization of seismically recorded infrasonic-acoustic signals to monitor volcanic explosions: The El Chichon Sequence 1982—A case study. Journal of Geophysical Research: Solid Earth, 88, 10,385–10,401, doi:10.1029/JB088iB12p10385.

McNutt, S. R. and E. R. Williams (2010). Volcanic lightning: global observations and constraints on source mechanisms, Bulletin of Volcanology, 72, 1153-1167.

Miller, S.D., Straka III, W., Mills, S.P., Elvidge, C.D., Lee, T.F., Solbrig, J., Walther, A., Heidinger, A.K., & Weiss, S.C. (2013). Illuminating the capabilities of the Suomi NPP VIIRS Day/Night Band. Remote SensIng, 5(12), 6717–6766. https://doi.org/10.3390/rs5126717

Miller, S. D., Straka, W. C., Yue, J., Smith, S. M., Alexander, M. J., Hoffmann, L., et al. (2015). Upper atmospheric gravity wave details revealed in nightglow satellite imagery. Proceedings of the National Academy of Sciences of the United States of America, 112(49), E6728–E6735. https://doi.org/10.1073/pnas.1508084112

Nakashima, Y., Heki, K., Takeo, A., Cahyadi, M. N., Aditiya, A., & Yoshizawa, K. (2016). Atmospheric resonant oscillations by the 2014 eruption of the Kelud volcano, Indonesia, observed with the ionospheric total electron contents and seismic signals. Earth and Planetary Science Letters, 434, 112–116. https://doi.org/10.1016/j.epsl.2015.11.029

Nelson, D.L., Garay, M.J., Kahn, R.A., & Dunst, B.A. (2013). Stereoscopic Height and Wind Retrievals for Aerosol Plumes with the MISR INteractive eXplorer (MINX). Remote Sensing, 5, 4593-4628, doi:10.3390/rs5094593.

Ogawa, T., Hiroshi Kumagai, K. Sinno (1982). Ionospheric disturbances over Japan due to the 18 May 1980 eruption of Mount St. Helens, J. Atmos. Terres. Physics, 44, 10, 863-868, https://doi.org/10.1016/0021-9169(82)90039-3.

Picone, J. M., Hedin, A. E., Drob, D. P., & Aikin, A. C. (2002). NRLMSISE-00 empirical model of the atmosphere: Statistical comparisons and scientific issues. *Journal of Geophysical Research*, **107**(A12), 1468. https://doi.org/10.1029/2002JA009430

Ripepe, M., De Angelis, S., Lacanna, G., & Voight, B. (2010). Observation of infrasonic and gravity waves at Soufrière Hills Volcano, Montserrat. Geophysical Research Letters, 37, L00E14, doi:10.1029/2010GL042557.

Ripepe, M., Barfucci, G., De Angelis, S., Delle Donne, D., Lacanna, G., & Marchetti, E. (2016). Modeling volcanic eruption parameters by near-source internal gravity waves. Scientific Reports, 36727.

Roberts, D. H., J. A. Klobuchar, P. F. Fougere, D. H. Hendrickson (1982a). A large-amplitude traveling ionospheric disturbance produced by the May 18, 1980, expkosion of Mount St. Helens, J. Geophys. Res., 87, A8, 6291-6301.

Roberts, D. H., A. E. E. Rogers, B. R. Allen, C. L. Bennett, B. F. Burke, P. E. Greenfield, C. R. Lawrence, T. A. Clark (1982b), Radio interferometric detection of a traveling ionospheric disturbance excited by the explosion of Mount St. Helens, J. Geophys. Res., 87, 48, 6302-6306.

Sentman, D. D., Wescott, E. M., Picard, R. H., Winick, J. R., Stenbaek-Nielsen, H. C., Dewan, E. M., Moudry, D. R., S ã o Sabbas, F. T., Heavner, M. J., & Morrill, J. (2003). Simultaneous observations of mesospheric gravity waves and sprites generated by a midwesterm thunderstorm, Journal of Atmospheric and Solar-Terrestrial Physics, 65, 537–550, doi:10.1016/S1364-6826(02)00328-0.

Shults, K., Astafyeva, E., & Adourian, S. (2016). Ionospheric detection and localization of volcano eruptions on the example of the April 2015 Calbuco events. Journal of Geophysical Research: Space Physics, 121, 10,303–10,315. https://doi.org/10.1002/2016JA023382

Smith, S. M., Setvak, M., Belesky, Y., Baumgardner, J., & Mendillo, M. (2020). Mesospheric gravity wave momentum flux associated with a large thunderstorm complex, Journal of Geophysical Research: Atmospheres, https://doi.org/10.1029/2020JD033381

Sugimoto, N., Fujisawa, Y., Kashimura, H., Noguchi, K., Kuroda, T., Takagi, M., & Hayashi, Y. (2021). Generation of gravity waves from thermal tides in the Venus atmosphere. Nature Communications, 12, 3682.

Suzuki, S., Shiokawa, K., Otsuka, Y., Ogawa, T., Nakamura, K., & Nakamura, T. (2007). A concentric gravity wave structure in the mesospheric airglow images. Journal of Geophysical Research: Atmospheres, 112, D02102, doi:10.1029/2005JD006558.

Tahira, M., Nomura, M., Sawada, Y., & Kamo, K. (1996). Infrasonic and acoustic-gravity waves generated by the Mount Pinatubo eruption of June 15, 1991, in Fire and Mud: Eruptions and Lahars of Mount Pinatubo, Philippines. Edited by C. G. Newhall and R. S. Punongbayan, pp. 601–614, Univ. of Wash. Press, Seattle.

Taylor, M. J., & Hapgood, M. A. (1988). Identification of a thunderstorm as a source of short period gravity waves in the upper atmospheric nightglow emissions. Planetary and Space Science, 36, 975– 985, doi:10.1016/0032-0633(88)90035-9.

533 Vadas, S. L., Yue, J., & Nakamura, T. (2012). Mesospheric concentric gravity waves generated
534 by multiple convective storms over the North American Great Plain. Journal of Geophysical
535 Research: Atmospheres, 117. https://doi.org/10.1029/2011JD017025
536
537 Widmer, R., & Zurn, W. (1992). Bichromatic excitation of long-period Rayleigh and air waves
538 by the Mount Pinatubo and El Chichon volcanic eruptions. Geophysical Research Letters, 19, 8,
539 765-768.
540
541 Yue, J., Vadas, S. L., She, C.-Y., Nakamura, T., Reising, S. C., Liu, H.-L., Stamus, P., Krueger,
542 D. A., Lyons, W., & T. Li (2009). Concentric gravity waves in the mesosphere generated by
543 deep convective plumes in the lower atmosphere near Fort Collins, Colorado, Journal of
544 Geophysical Research: Atmospheres, 114, D06104, doi:10.1029/2008JD011244.
545
546 Yue, J., Miller, S., Hoffmann, L., & Straka III, W. C. (2014). Stratospheric and mesospheric
547 concentric gravity waves over tropical cyclone Mahasen: Joint AIRS and VIIRS satellite
548 observations. Journal of Atmospheric and Solar-Terrestrial Physics, 119, 83-90,
549 doi:10.1016/j.jastp.2014.07.003.
550
551 Yue, J., Perwitasari, S., Xu, S., Hozumi, Y., Nakamura, T., Sakanoi, T., Saito, A., Miller, S. D.,
552 Straka, W., & Rong, P. (2019). Preliminary dual-satellite observations of atmospheric gravity
553 waves in airglow: ISS-IMAP VISI vs. Suomi NPP VIIRS DNB. Atmosphere, 10, 650,
554 doi:10.3390/atmos10110650.
555

Figure 1. (a) MISR stereo-derived plume-height map showing the La Soufriere eruption plume at ~1435 UT on April 10, 2021. (b) Downwind profile plot of the same plume. Red points are derived from the parallax of plume contrast elements in the MISR multi-angle imagery; blue points present the heights corrected for any proper motion of plume elements. The surface elevation is indicated in green.

Figure 2. GOES-16 ABI infrared observations of the volcanic plume on April 11 2021, along with a GLM lightning detection (blue flash) at 0510 UT (lower left panel).

Figure 3. Thermal IR (11 um; top panels) and Day Night Band (bottom panels) VIIRS observations of volcanic plume and airglow gravity waves at 0516 UT (SNPP spacecraft; left panels) and 0606 UT (NOAA-20; right panels) on April 11 2021. The white lines denote the bright gravity wave fronts.

Figure 4. (a-d) Two-dimensional filtered GNSS TEC maps with the Butterworth band-pass filtering (10–30 min) indicating the CVIDs after the La Soufriere volcanic eruption on April 11 2021. The red dashed circles help to locate those concentric CVIDS over Cuba.
(e) Keogram of the CVIDs. The vertical axes are great circle distances between each of SIPs of filtered TEC and the position of the La Soufriere volcanic. The slant dashed lines denote the propagation velocities of the CVIDs.

Figure 1.

(a)

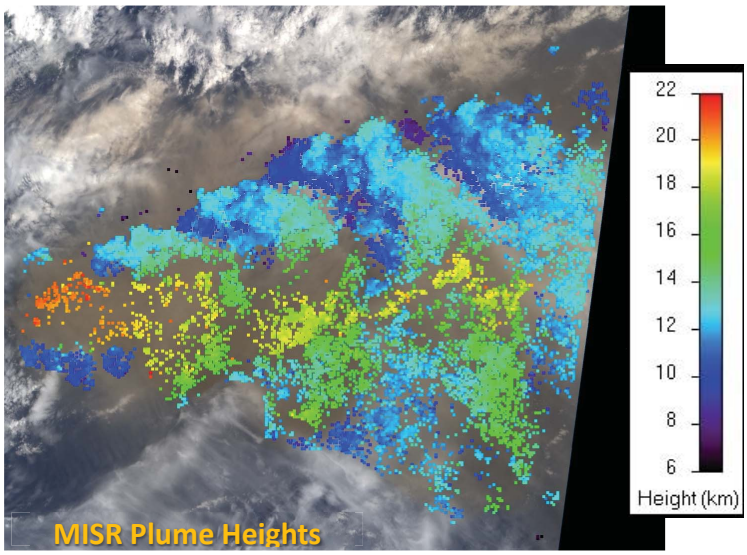
22
20
18
16
14
12
10
8
6
Height (km)
MISR Plume Heights

(b)

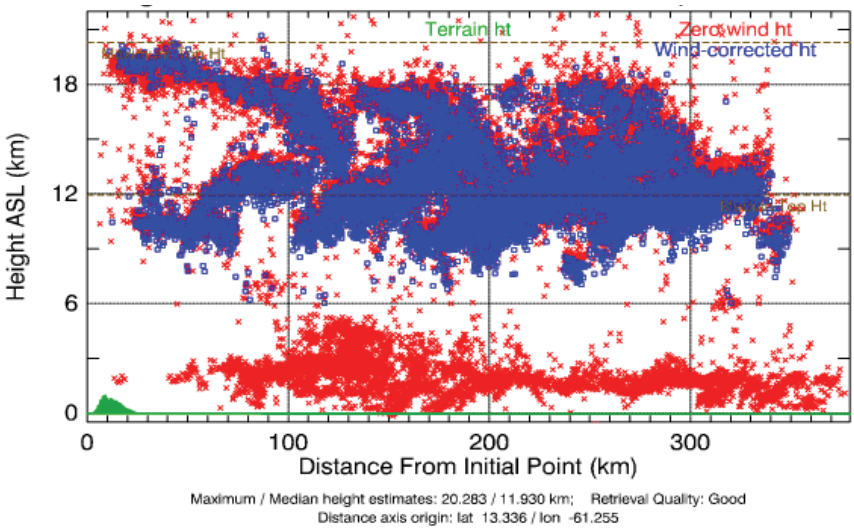
Terrain ht
Zero-wind ht
Wind-corrected ht
18
12
6
0
Height ASL (km)
0
100
200
300
Distance From Initial Point (km)
Maximum / Median height estimates: 20.283 / 11.930 km; Retrieval Quality: Good
Distance axis origin: lat 13.336 / lon -61.255

Figure 2.

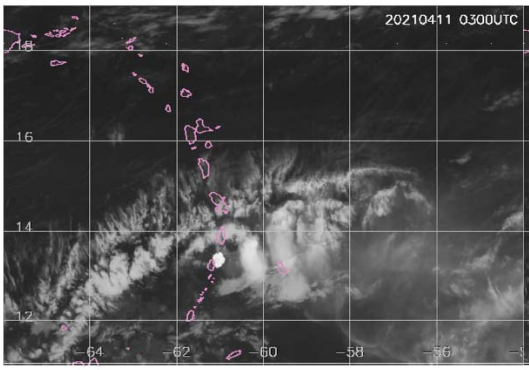
20210411 0300UTC
18
16
14
12
-64
-62
-60
-58
-56

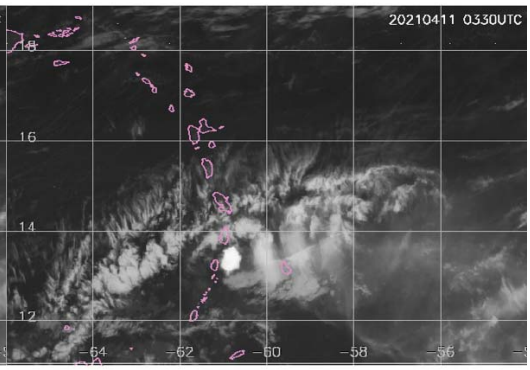
20210411 0330UTC
18
16
14
12
-64
-62
-60
-58
-56

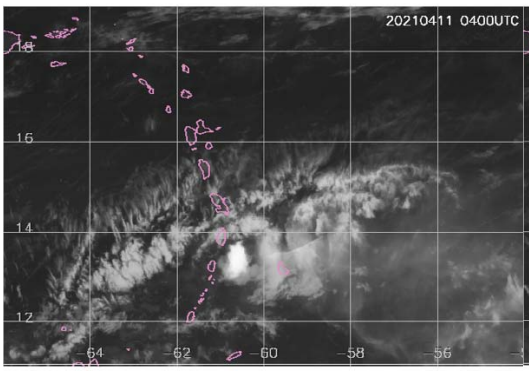
20210411 0400UTC
18
16
14
12
-64
-62
-60
-58
-56

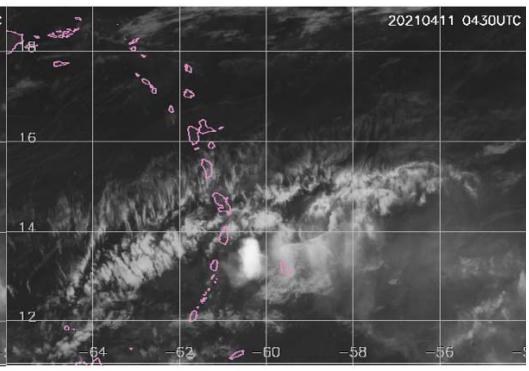
20210411 0430UTC
18
16
14
12
-64
-62
-60
-58
-56

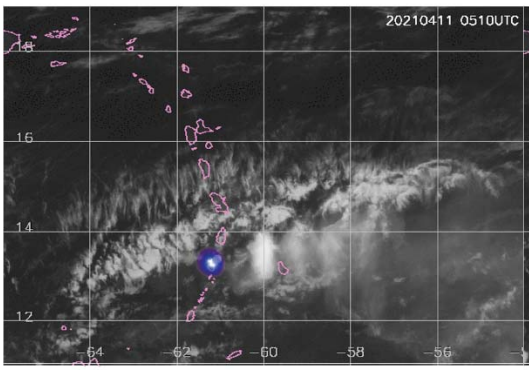
20210411 0510UTC
18
16
14
12
-64
-62
-60
-58
-56

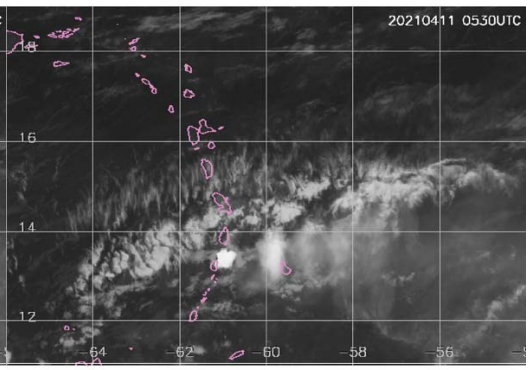
20210411 0530UTC
18
16
14
12
-64
-62
-60
-58
-56

Figure 3.

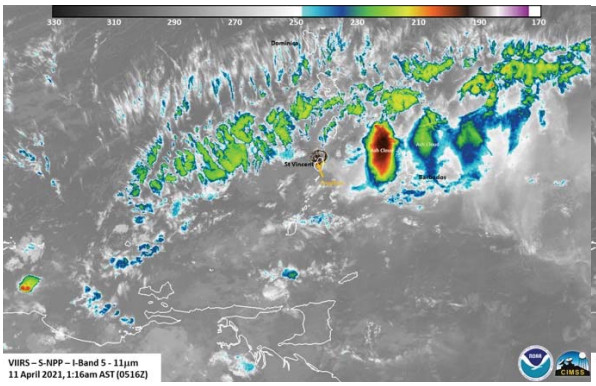
330 310 290 270 250 230 210 190 170
Dominica
St Vincent
Barbados
VIIRS – S-NPP – I-Band 5 - 11µm
11 April 2021, 1:16am AST (0516Z)

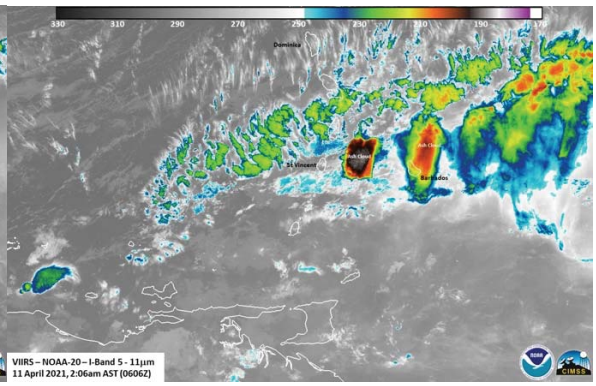
330 310 290 270 250 230 210 190 170
Dominica
St Vincent
Barbados
VIIRS – NOAA-20 – I-Band 5 - 11µm
11 April 2021, 2:06am AST (0606Z)

d

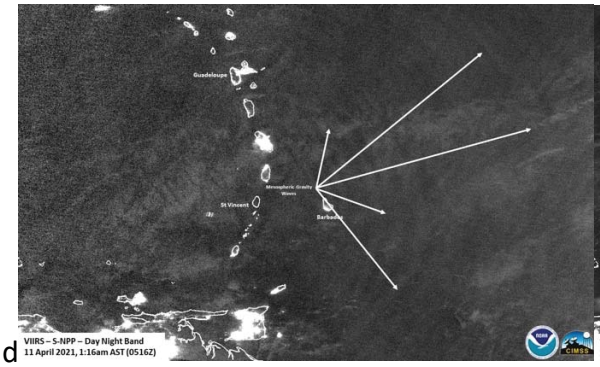
Guadeloupe
Monserrat
St Vincent
Barbados
VIIRS – S-NPP – Day Night Band
11 April 2021, 1:16am AST (0516Z)

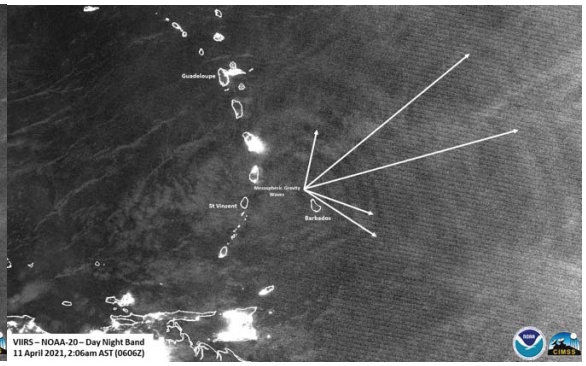
Guadeloupe
Monserrat
St Vincent
Barbados
VIIRS – NOAA-20 – Day Night Band
11 April 2021, 2:06am AST (0606Z)

Figure 4.

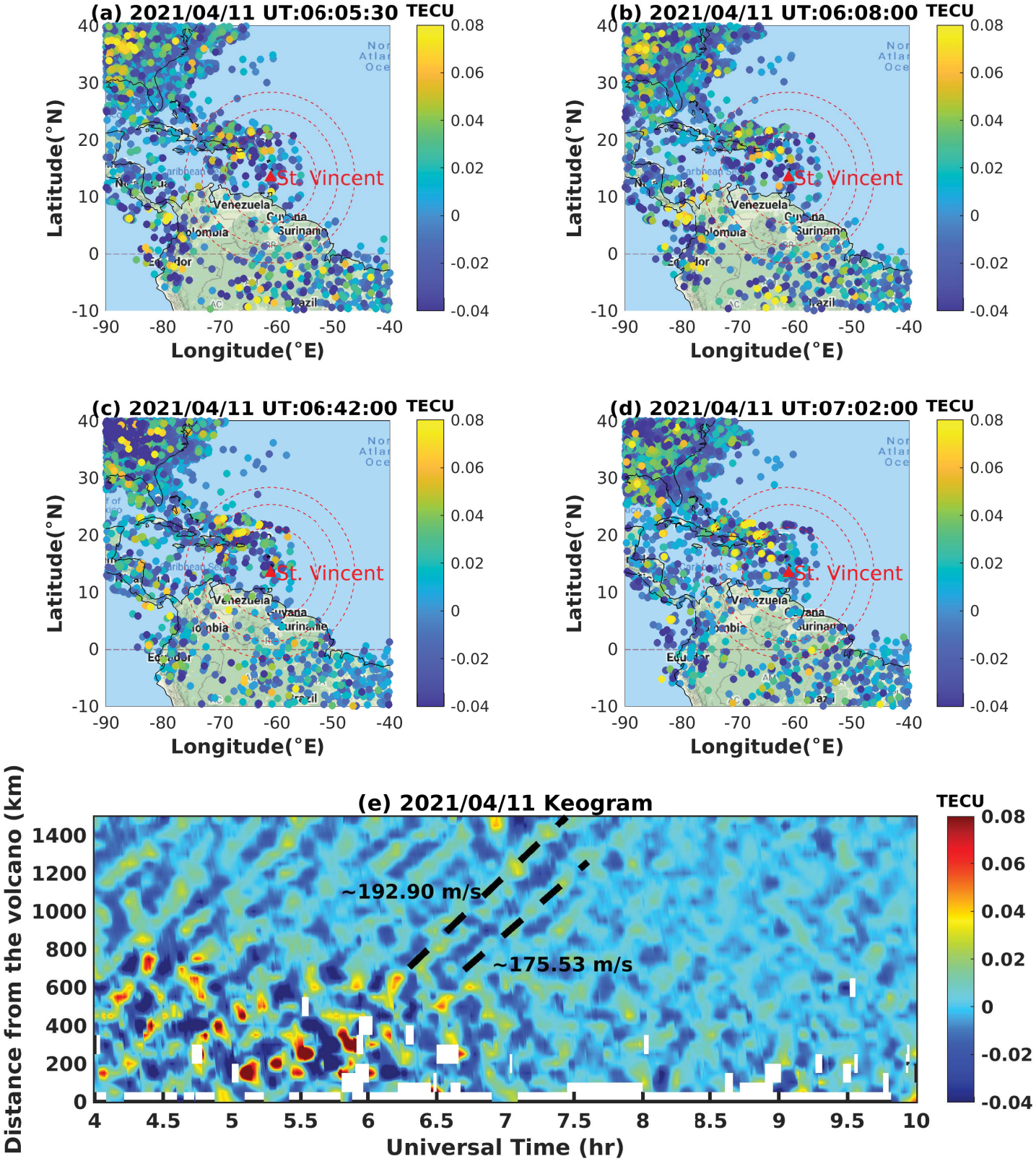
(a) 2021/04/11 UT:06:05:30
(b) 2021/04/11 UT:06:08:00
(c) 2021/04/11 UT:06:42:00
(d) 2021/04/11 UT:07:02:00
TECU
0.08
0.06
0.04
0.02
0
-0.02
-0.04
St. Vincent
Venezuela
Guyana
Suriname
Latitude(°N)
Longitude(°E)
40
30
20
10
0
-10
-90
-80
-70
-60
-50
-40
(e) 2021/04/11 Keogram
~192.90 m/s
~175.53 m/s
Distance from the volcano (km)
1400
1200
1000
800
600
400
200
0
4
4.5
5
5.5
6
6.5
7
7.5
8
8.5
9
9.5
10
Universal Time (hr)